RICE UNIVERSITY

FlatCam: Lensless Imaging, Principles, Applications and Fabrication

by

Ali Ayremlou

A Thesis Submitted
in Partial Fulfillment of the
Requirements for the Degree

Master of Science

Approved, Thesis Committee:

Richard G. Baraniuk, Chair
Victor E. Cameron Professor of Electrical and Computer Engineering

Ashok Veeraraghavan
Assistant Professor of Electrical and Computer Engineering

Jacob T. Robinson
Assistant Professor of Electrical and Computer Engineering

Houston, Texas

December, 2015

RICE UNIVERSITY

FlatCam: Lensless Imaging, Principles, Applications and Fabrication

by

Ali Ayremlou

A Thesis Submitted
in Partial Fulfillment of the
Requirements for the Degree

Master of Science

Approved, Thesis Committee:

Richard G. Baraniuk, Chair
Victor E. Cameron Professor of Electrical
and Computer Engineering

Ashok Veeraraghavan
Assistant Professor of Electrical and
Computer Engineering

Jacob T. Robinson
Assistant Professor of Electrical and
Computer Engineering

Houston, Texas

December, 2015

ABSTRACT

FlatCam: Lensless Imaging, Principles, Applications and Fabrication

by

Ali Ayremlou

FlatCam is a thin form-factor camera that consists of a coded mask placed on top of a bare, conventional sensor array. The design is inspired by coded aperture imaging principles, each sensor pixel records a linear combination of the scene in front of the camera, and a computational algorithm reconstructs the image. A key design feature of the FlatCam is its slim form-factor, which enables imaging using extremely thin, even flexible surfaces that operate over a wide spectral range and are amenable to monolithic fabrication. The potential of FlatCam design is demonstrated in two scenarios utilizing two separate prototypes: one at visible wavelengths and the other at infrared wavelengths.

Contents

Abstract ii

List of Illustrations iv

1 Introduction 1

1.1 Related work 4

2 Lensless Imaging Principles 7

2.1 Mask Design 7

2.2 Calibration 10

2.3 Reconstruction 11

3 Applications and Experimental Results 13

3.1 Visible Light 15

3.2 Infrared 16

4 Prototype and Fabrication 18

4.1 Prototype 18

5 Conclusion 20

Bibliography 21

/Users/Ali/Dropbox/MS Thesis/chapter1.tex

Illustrations

1.1 FlatCam architecture 3

2.1 M-sequences masks 8
2.2 Visible FlatCam prototype and results 9
2.3 Calibration 11

3.1 Real scene reconstructions 13
3.2 Monitor image reconstructions 14
3.3 Video results 16
3.4 SWIR FlatCam prototype and results 17

Chapter 1

Introduction

Sometimes, size does matter. A range of new imaging applications is driving the miniaturization of cameras and imaging systems. Good progress has been made in one direction, namely minimizing the total volume of the camera, which has enabled new applications in endoscopy, pill cameras, and in vivo microscopy. Unfortunately, this strategy of miniaturization has an important shortcoming: the amount of light collected, which is directly proportional to the area of the photosensitive material, also decreases dramatically. As a consequence, ultra-small imagers built simply by scaling down the optics and sensors suffer from extremely low light collection.

Only limited progress has been made in the other direction of miniaturization, namely minimizing the thickness of the camera while still preserving its ability to utilize a large sensor surface area. Such a design would support imagers that can be distributed over large and even flexible surfaces, such as credit cards, wallpaper, and clothing, resulting in a number of novel applications.

In this paper, we present FlatCam, an imaging architecture that enables the use of a very large photosensitive area with a very thin form factor. This is the distinguishing feature which bears the hallmark of our design. The FlatCam achieves its thin form factor by dispensing with a lens and replacing it with a coded mask placed almost immediately atop a bare conventional sensor array. For a given thickness constraint, a FlatCam enables the use of an order of magnitude larger sensor compared to a minimum volume camera, resulting in two orders of magnitude improvement

in light collection. Furthermore, a FlatCam is amenable to direct fabrication using conventional techniques while operating over a wide spectral range. Our design uses a computational algorithm to recover the image from the sensor measurements.

An illustration of the FlatCam design is presented in Fig. 1.1. Light from the scene passes through a coded mask and lands on a conventional image sensor. The mask consists of opaque and transparent features (to block or transmit light, respectively) that can be viewed as pinholes arranged in a carefully designed pattern. Light from each focal plane region falls on a unique collection of pixels in the sensor, and this mapping can be represented using a linear operator. A computational algorithm then inverts this linear operator to recover the original light distribution of the scene.

The FlatCam's departure from a lens-based architecture addresses some of the key limitations of the latter. First, while image sensors are typically thin, lens-based cameras end up being thick because of the lens complexity and the large distance required between the lens and sensor to achieve focus. Furthermore, the camera's thickness increases as the sensor and the lens aperture sizes increase. Second, while Moore's Law has cut the cost of digital image sensors exponentially over time, lenses do not benefit from this exponential scaling, particularly at wavelengths farther into the infrared and ultraviolet spectra, where inexpensive glass and plastics cannot be used. Third, lens-based cameras invariably require post-fabrication assembly, resulting in manufacturing inefficiencies.

Imaging without a lens is not an entirely new idea. Pinhole cameras, the progenitor of lens-based cameras, have been well known since Alhazen (965–1039AD) and Mozi (c. 370BCE). However, a tiny pinhole drastically reduces the amount of light reaching the sensor, resulting in noisy, low-quality images. Indeed, lenses were introduced into cameras for precisely the purpose of increasing the size of the aperture, and thus the

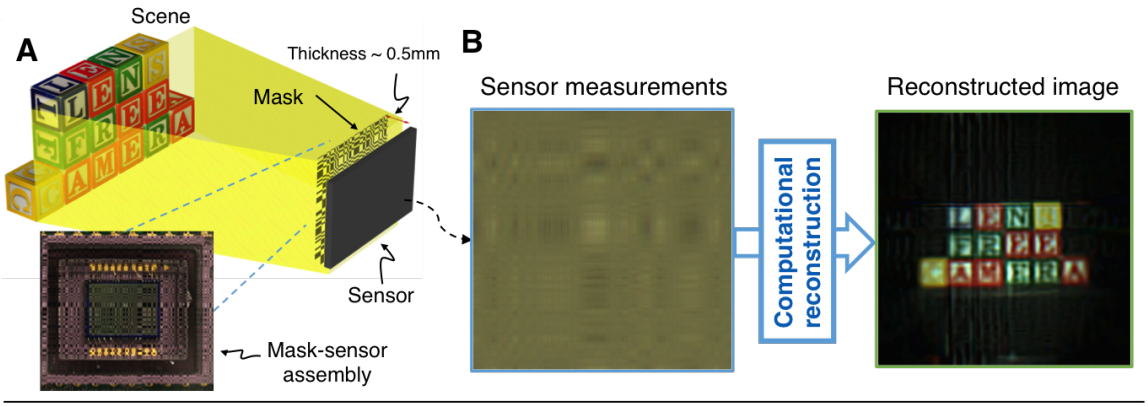

Light throughput	Low (~F/22)	High (~F/1.8)	High (~F/2.54)
Fabrication	Requires post-fabrication	Requires post-fabrication	Direct fabrication
Thickness	~10-20mm	~10-20mm	~10-500μm
Infrared and thermal	No wavelength limitations	Costly optics	No wavelength limitations
Cost	$	$$	$
Curved or flexible geometries	Infeasible due to limited field of view	Infeasible due to rigid optics	Adaptable to curved and flexible sensors

Figure 1.1 : FlatCam architecture. **(A)** shows the mask-sensor assembly of our prototype. **(B)** An example of sensor measurements and the image reconstructed by solving a computational inverse problem. **(C)** Comparison of pinhole, lens-based, and FlatCam cameras.

light throughput, without degrading the sharpness of the acquired image.

Our FlatCam design can be interpreted as an extension of the pinhole camera but with a multitude of pinholes operating in parallel [1, 2]. Such systems are typically referred to as coded aperture cameras [3, 4, 5, 6, 7, 8] and are commonly used in x-ray and gamma-ray imaging [9, 10, 11, 12]. The primary goal of these designs has been to increase the light throughput compared to a pinhole camera, but the resulting cameras invariably remain thick. In contrast, our FlatCam design offers a thin form factor. For instance, in our prototype with a visible sensor, the spacing between the

sensor and the mask is only 0.5mm.

Our FlatCam design has many attractive properties besides its slim profile. First, since it minimizes the thickness of the camera but not the area of the sensor, it collects more light than low-volume cameras, leading to higher quality imagery. Second, the mask can be created from inexpensive materials that operate over a broad range of wavelengths. Third, the mask can be fabricated simultaneously with the sensor array, creating new manufacturing efficiencies. The mask can be fabricated either directly in one of the metal interconnect layers on top of the photosensitive layer, or on a separate wafer thermal compression that is bonded to the back side of the sensor, as is typical for back-side illuminated image sensors [13]. Fig. 1.1 summarizes some salient features of pinhole, lens-based, and FlatCam architectures.

We will go through the principles behind the scene for lensless imaging in Chapter 2 and will demonstrate the potential of the FlatCam using two prototypes: a visible prototype in which the mask-sensor spacing is 0.5mm and a short-wave infrared (SWIR) prototype in which the spacing is about 5mm in Chapters 3 and 4.

1.1 Related work

A number of thin imaging systems have been developed over the last few decades. The TOMBO architecture [14], inspired by insect compound eyes, reduces the camera thickness by replacing a single, large focal-length lens with multiple, small focal-length microlenses. Each microlens and the sensor area underneath it can be viewed as a separate low-resolution, lens-based camera, and a single high-resolution image can be computationally reconstructed by fusing all of the sensor measurements. Similar architectures have been used for designing thin infrared cameras [15]. The camera

thickness in this design, the thickness of the camera is dictated by the geometry of the micro-lenses used. Thus, reducing the camera thickness requires a proportional reduction in the sizes of the microlenses and sensor pixels. As a result, microlens-based cameras currently offer only up to a four-fold reduction in the camera thickness [16, 17].

An alternate approach for achieving thin form factors relies on folded optics, where light manipulation similar to that of a traditional lens is achieved using multi-fold reflective optics [18]. However, folded optics based systems have low light collection efficiencies.

Recently, miniature cameras with integrated diffraction gratings and CMOS image sensors have been developed [19, 20, 21, 22]. These cameras have been successfully demonstrated on specific tasks such as motion estimation and face detection. While these cameras are indeed ultra-miniature in total volume (100 micron sensor width by 200 micron thickness), they retain the large thickness-to-width ratio of conventional lens-based cameras. Moreover, because of the small sensor size, they suffer from reduced light collection ability. In contrast, in our visible prototype below, we used a 6.7mm wide square sensor, which increases the amount of light collection by about three orders of magnitude, while the device thickness remains approximately similar (500 micron).

An on-chip, lens-free microscopy design that uses amplitude masks to cast a shadow of point illumination sources onto a microscopic tissue sample has shown significant promise for microscopy and related applications, where the sample being imaged is very close to the sensor (less than 1mm) [23, 24]. Unfortunately, this technique cannot be directly extended to traditional photography and other applications that require greater standoff distances and do not provide control over illumination.

Coded-aperture systems have traditionally been used for imaging wavelengths beyond the visible spectrum, for which lenses or mirrors are expensive or infeasible. In recent years, coded aperture-based systems using compressive sensing principles [25, 26, 27] have been studied for image super-resolution [28], spectral imaging [29], and video capture [30]. Mask-based lens-free designs have also been proposed for flexible field-of-view selection [31], for compressive single-pixel imaging using a transmissive LCD panel [32], and for separable coded masks [33]. In these designs, the distance between the image sensor and the mask is too great (in the 5–10mm range) to provide thin form factor capabilities, which is the key focus of our work.

Chapter 2

Lensless Imaging Principles

In this chapter we will cover some principles behind lensless imaging and analyze the necessary pre and post processes for capturing using FlatCam. Lensless imaging consist of a binary mask placed in a specific distance from sensor d as shown in Fig. 2.2 parallel to it. Assuming sensor size to be $M \times M$, the pixel measurements can be noted with a vector y of size M^2. On the other hand planar scene's pixel values can be represented with a $N \times N$ matrix or equivalently with a N^2 vector x. Using this model, lensless imaging systems can be simply represented with following equation due to its linearity:

$$y = \Phi x + n \tag{2.1}$$

where the multiplexing matrix Φ is a $M^2 \times N^2$ matrix that its structure is all dependent on mask to sensor distance, mask feature size and some more complicated physical features of the system. Here, n is an additive noise that is due to the sensor noise and non-idealities of the system.

2.1 Mask Design

It is inevitable that the structure and pattern of the mask should play the main role in this system; and therefore, they have to be selected carefully. For this purpose, we have chosen m-sequence patterns for our system, due to its flat spectral properties

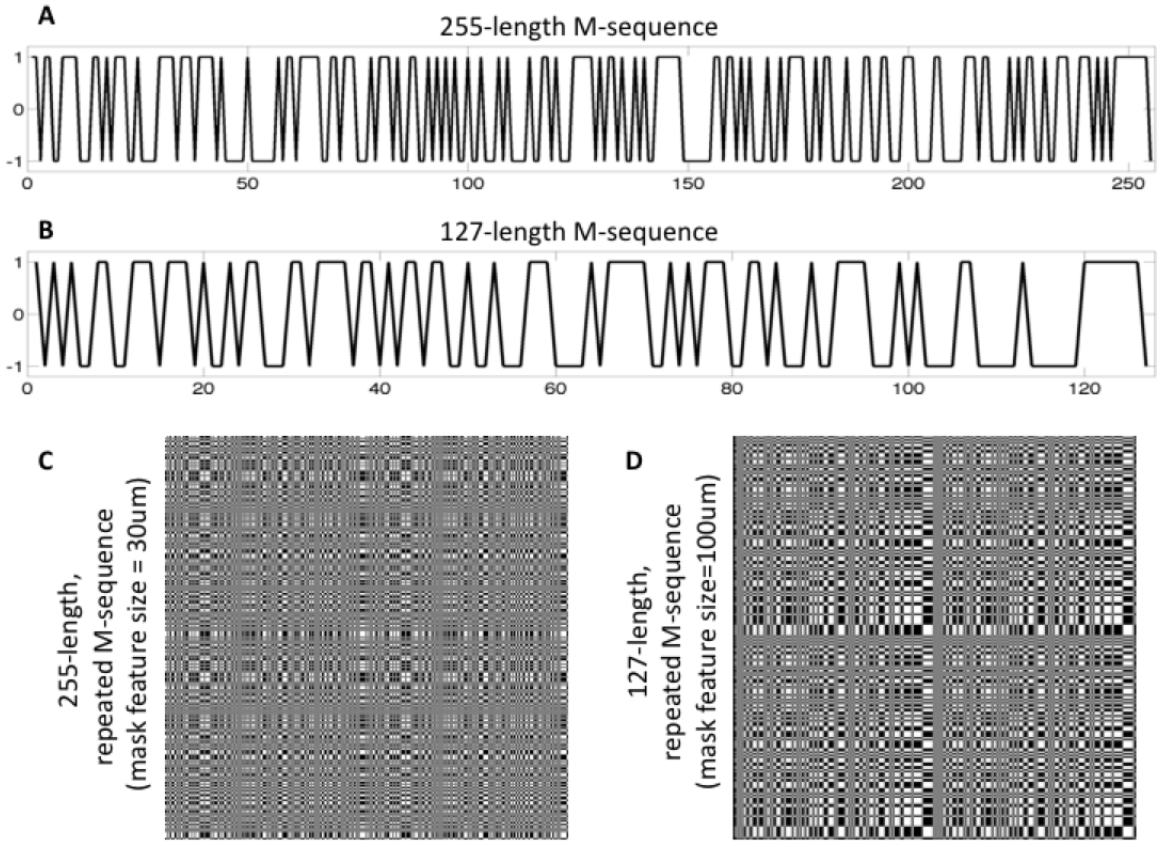

Figure 2.1 : M-sequences masks. Masks used in both our visible and SWIR prototype lens-free cameras. M-sequences with ± 1 entries that we used to create the binary masks for **(A)** the visible camera and **(B)** the SWIR camera. Binary masks created from the M-sequences for **(C)** the visible camera and **(D)** the SWIR camera

[34], that are 1D patterns. An example of 127 and 255 m-squences are depicted in Fig. 2.1. To make 2D binary masks using these patterns we have done cross production of the pattern with itself, which extends all desirable properties of 1D m-sequence patterns to the second dimension. 2.1 shows examples of 2D patterns that we have been used in our system.

According to equation 2.1, the huge size of multiplexing matrix Φ, $M^2 \times N^2$, can slow down many processes for calibration and reconstruction due to high complexity,

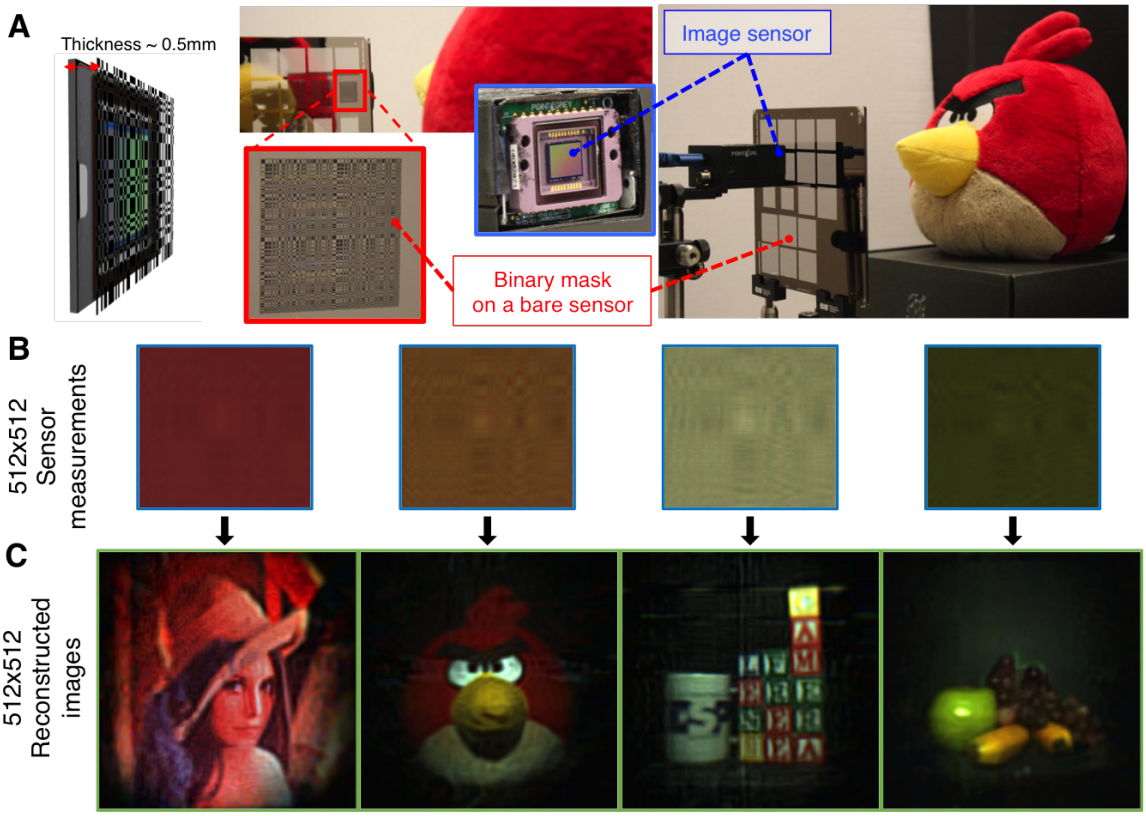

Figure 2.2 : Visible FlatCam prototype and results. **(A)** Prototype consists of a the sensor with a separable M-sequence mask. **(B)** The sensor measurements. **(C)** Reconstructed 512×512 color images. Processing was performed for each color channel independently.

and consequently make the system's utilization impractical. One of the hacks to lower the complexity is to use a separable mask. Assuming a separable mask, the system modeling can be re-rewitten as follow:

$$Y = \Phi_L X \Phi_R^T + N \tag{2.2}$$

where Φ_L and Φ_R^T are 1D convolutions along rows and columns of the scene $M \times M$ pixels matrix X, that produce $N \times N$ sensor measurement matrix. This reformation in modalization reduces the complexity of multiplexing matrices to $2MN$, whereas it was M^2N^2 in the classic equation. The utilization of a separable mask to reduce

complexity, which has never been done before, gives the most novelty to our lensless imaging system. In following section, our approach to computing the multiplexing matrices and recovering scene image using them will be explained.

2.2 Calibration

To complete our model of the system based on equation 2.2 and consequently invert the system for image recovering, we need to fill two more unknowns in the equation, Φ_L and Φ_R^T. These parameter can be either calculated analytically according to physical parameters of system, or calibrated using known inputs and outputs of the system. Due to non-ideality of the system and various complicated physical phenomena, deriving an accurate analytical model is not feasible, nor stable, yet, because of lacking the exact parameters of the physical phenomena. Therefore, we have chosen the practical calibration approach.

Simply, calibration can be performed by sweeping an all ones vector along rows and columns of the X matrix, inverting the systems and then extracting Φ_L and Φ_R^T matrices. However, in practice, this is equal to sweeping a line of light horizontally and vertically, and respectively capturing Y measurements off the sensor. The problem with this approach, however, is low light throughput and, consequently, high level of noise, that would reduce accuracy in system inversion.

To overcome this problem, instead of a single line of light, combinations of these lines has to be utilized to increase the light throughput. One approach that we have chosen, was using Hadamard codes instead. Hadamard codes always consist of half of the size ones and half zeros, this means increasing the light throughput to 50% rather than $1/M$.

Solving the major obstacles, calibration process in practice is straightforward. As

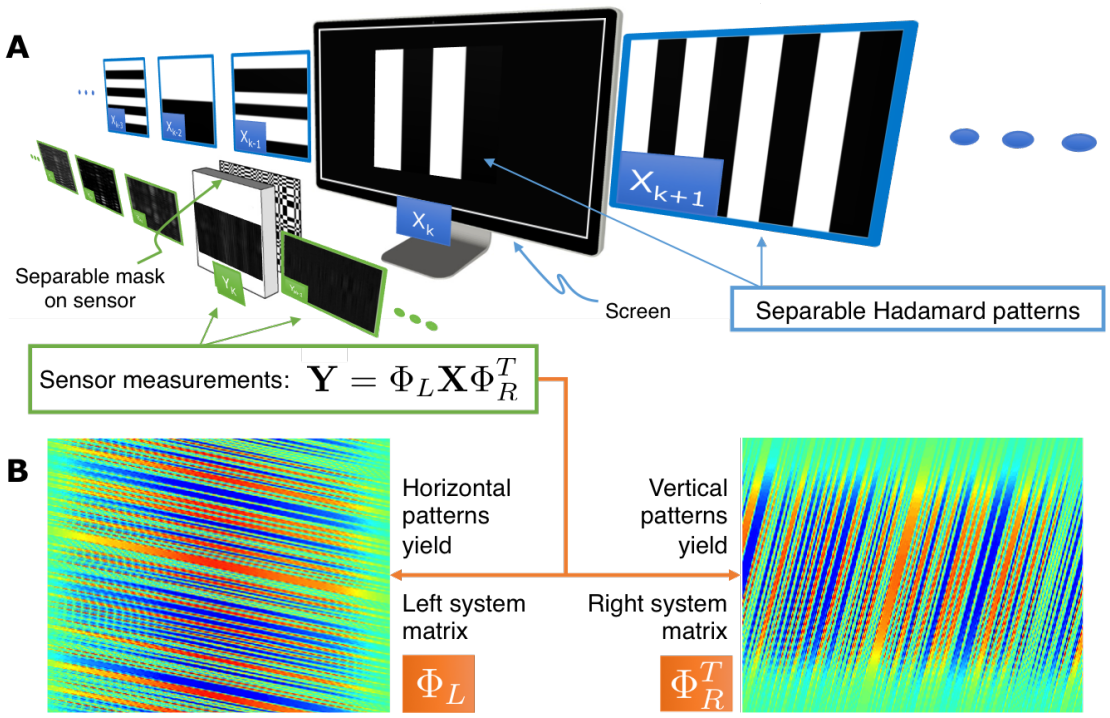

Figure 2.3 : Calibration for measuring the left and right multiplexing matrices Φ_L and Φ_R. **(A)** We display special separable patterns on a computer screen for the visible camera and on a diffused screen using a projector for the SWIR camera. The sensor measurements recorded from these stripe patterns are re-ordered to form the left and right multiplexing operators shown in **(B)**.

input (X) to the system, Hadamard codes have to be fed to the system and corresponding outputs (Y) have to be measured and stored (Fig. 2.3). Having all these measurements, the system can be inverted which will be discussed in next section.

2.3 Reconstruction

Continuing from equation 2.2 and considering calculated multiplexing matrices using calibration, the system can be solved by the least square estimation methods [35]:

$$\min_X ||Y - \Phi_L X \Phi_R^T||_2^2 \tag{2.3}$$

and get an estimate for scene pixels X. However, because of multiplexing matrices Φ_L and Φ_R not being well-conditioned, the least square methods will suffer from noise amplification. To eliminate this issue a regularization factor has to be introduced to the problem:

$$\min_X ||Y - \Phi_L X \Phi_R^T||_2^2 + \lambda f(X) \tag{2.4}$$

In 2.4, $f(.)$ could be any penalty function with a proper behavior that would be minimized for a better estimation. Among the most general regularization factors, TV(Total Variation)[36], Wavelets[37] and l_2-regularized are widely used for image recovering purposes. In our cases, we have utilized all these regularization functions and which are compared in figures 3.2 and 3.1. In our experience, l_2-regularization showed better performance for our purpose, accounting complexity and quality. Fig. 2.3 demonstrates this process with actual results from our experiments.

Chapter 3

Applications and Experimental Results

Due to its thin structure and high level of light throughput, FlatCam can lead into many applications in medical, industrial, and everyday lifestyle fields. Besides, the absence of lens gives the opportunity to develop a flexible lensless camera. In general, the thickness factor in many electronic devices, such as smartphones, tablets, med-

Figure 3.1 : Images of real objects reconstructed at 512×512 resolution using three methods. **(A)** SVD-based solution of (8). **(B)** SVD solution followed by denoising with BM3D. **(C)** Total variation minimization using TVAL3 solver.

Figure 3.2 : Test images reconstructed at 512×512 resolution using the visible lensless camera prototype and three different reconstruction methods. **(A)** Original images. **(B)** SVD-based solution. **(C)** SVD/BM3D reconstruction. **(D)** Total variation (TV) based reconstruction.

ical in-place imaging and regular digital camera, is dictated with camera module's thickness. Cutting the thickness of the current camera modules into, at least, half can revolutionize these industries.

In addition to thickness, for some ranges of frequencies like ultra-violet or infrared, lenses are either very rare and expensive or infeasible. FlatCam gives us the oppor-

tunity to extend imaging to wider range of frequencies. In section 3.2, experimental results for a near infrared imaging system will be discussed. On the other hand, one of the most important advantages that FlatCam offers is cost reduction as a heavy cost factor, i.e. lens, is eliminated..

In the next sections, experimental results for visible and infrared applications plus a list of some potential areas of applications will follow.

3.1 Visible Light

In this experiment, a binary mask with M-sequence has been placed in the nearest possible distance from the sensor. After calibration and necessary adjustment using a monitor in a specific distance from camera, the system was put to test using sample images displayed on monitor as well as real objects placed at the same depth illuminated by a desk lamp. As discussed in section 2.3, the captured images had to be reconstructed which was done in a fraction of second and the resulting images are shown in Fig. 3.1 and Fig. 3.2.

The lensless setup for visible light imaging gave us a fair quality, and the whole process was done very short amount of time, both of which were indications that the system could be extended to video capturing as well. In the video experiment, we used the same setup, but this time a 30fps video was shot. After post processing, reconstruction and denoising, the resulting video had the same quality as that of the images. Some sample frames of this experiment are shown in Fig. 3.3.

This experiment is an evidence to prove that lensless imaging can be utilized in one of the most popular areas of application in life, visible light imaging. The system makes possible the development of cameras as thin as credit cards, wearable cameras

(for use in sports and other action packed activities), flexible cameras with a a wide FOV, and many more applications that we may or may not be aware of since we did not possess the tool that could get the job done until today.

3.2 Infrared

Lensless imaging can be easily extended to another range of light without violating its principals. One of these areas is near infrared imaging that has many applications in medical science, military and everyday life. For this experiment we used a Short Wave Infrared (SWIR) camera that had a 256×300 resolution, but due to the limitation in reaching close to the sensor our capturing resolution and consequently reconstructed image resolution was limited to 64×64. We used the same mask ex-

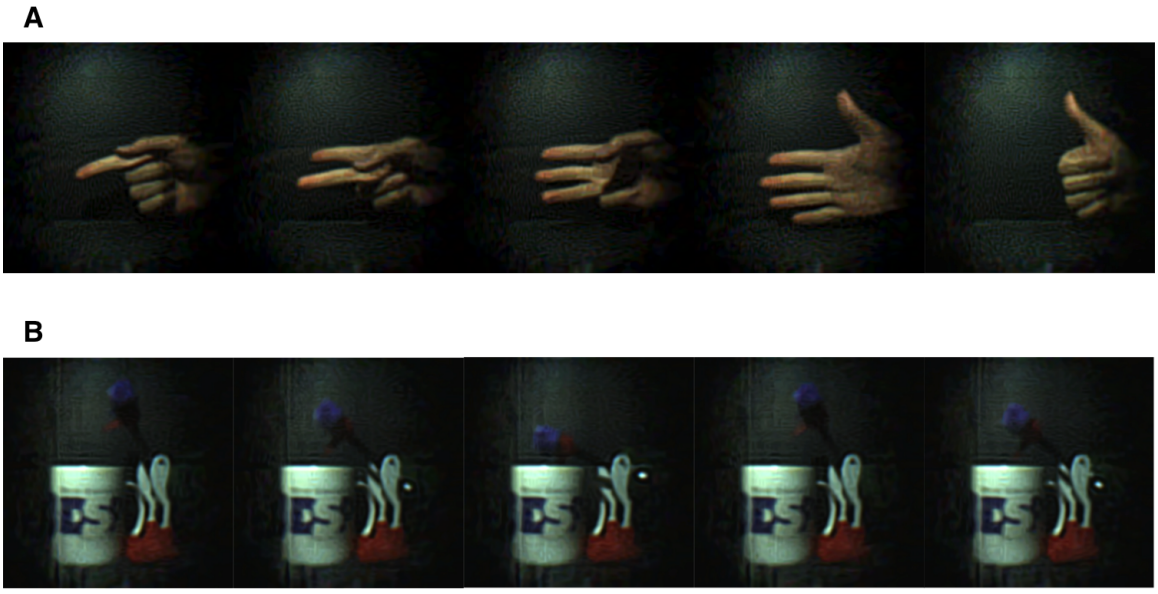

Figure 3.3 : Dynamic scenes captured at video rates and reconstructed at 512×512 resolution. **(A)** Frames from the video of a gesturing hand captured at 30 frames per second. **(B)** Frames from the video of a toy bird captured at 10 frames per second.

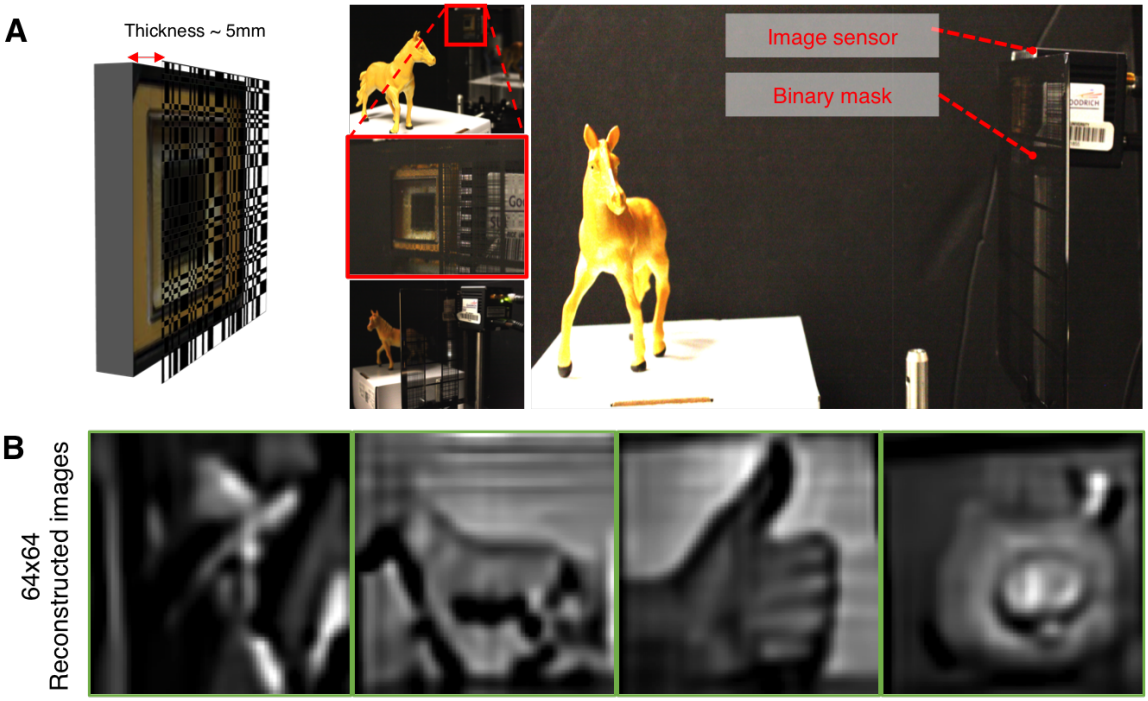

Figure 3.4 : Short wave infrared (SWIR) FlatCam prototype and results. **(A)** Prototype consists of a Goodrich 320KTS-1.7RT sensor with a separable M-sequence mask placed approximately $5mm$ from the detector surface. **(B)** Reconstructed 64×64 images.

plained in section 3.1.

Calibration and post processing procedure is similar to visible light imaging; in fact, this is constant for any range of lensless imaging. The system was tested only on monitor images and real objects; the setup and the results are depicted in Fig. 3.4.

Chapter 4

Prototype and Fabrication

One of the greatest advantages of lensless imaging system is its simple and easy manufacturing procedure. Simply, a lensless camera can be made from a sensor, a proper binary mask plus the necessary pre/post computations, in comparison to lens-based cameras that have a more complex fabrication process, especially if more than one lens is going to be involved in the system. In this chapter, we will explain how a lensless camera prototype can be made from readily available, on-the-shelf devices, and what are the necessary procedures.

4.1 Prototype

This prototype has been made for our experiments and its results have been discussed in section 3.1. As mentioned before and depicted in Fig. 1.1, the lensless camera consists of two parts: a sensor and a mask. The sensor selection is very dependent to the application and there is no limitation in choosing different sensors for various wavelengths. We have chosen Sony ICX285 due to its $6.45\mu m$ pixel size and its consequent good noise profile. And for the mask, we used a photomask with binary m-sequence pattern with $30\mu m$ feature size.

Having sensor and mask properly selected, the mask has to be placed in parallel to sensor surface within a suitable distance. The most important factor in finding the

best distance that has to be considered is diffraction blur size that has to be smaller than pixel or the pix el patch size. Since there was a hot mirror placed on the top which was limiting us in getting closer to the sensor, had to be placed our mask $500\mu m$ from the sensor and this was making the blur size larger than a single pixel size; therefore, we had to patch pixels into 2x2 patches in order to overcome diffraction blur size.

The mask has to be completely aligned with the sensor in all directions. For that purpose, we found the placing of two single bars, one horizontal and the other vertical, on the monitor very helpful. The monitor that is used for calibration has to be aligned both with the sensor and the mask as well.

As discussed in sections 2.2 and 2.3, next steps would be calibration with Hadamard codes, inverting the imaging system, capturing real scenes and reconstructing scene images using matrices computed from the calibration process.

Chapter 5

Conclusion

The mask-based, lens-free FlatCam design proposed here has the potential to revolutionize an important emerging area of imaging, since high-performance, broad-spectrum cameras can be monolithically fabricated instead of requiring cumbersome post-fabrication assembly. The thin form factor and low cost of lens-free cameras makes them ideally suited for many applications in surveillance, large surface cameras, flexible or foldable cameras, disaster recovery, and beyond, where cameras are either disposable resources or integrated in flat or flexible surfaces and therefore have to satisfy strict thickness constraints. Emerging applications like wearable devices, internet-of-things, and in-vivo imaging could also benefit from the FlatCam approach.

Bibliography

[1] M. S. Asif, A. Ayremlou, A. Sankaranarayanan, A. Veeraraghavan, and R. Baraniuk, "Flatcam: Thin, bare-sensor cameras using coded aperture and computation," *Computational Imaging, IEEE Transactions on*, 2015.

[2] M. S. Asif, A. Ayremlou, A. Sankaranarayanan, A. Veeraraghavan, and R. Baraniuk, "Flatcam: Replacing lenses with masks and computation," in *Computer Vision Workshops (ICCV Workshops), 2015 IEEE International Conference on*, IEEE, 2015.

[3] R. Dicke, "Scatter-hole cameras for x-rays and gamma rays," *The Astrophysical Journal*, vol. 153, p. L101, 1968.

[4] E. Fenimore and T. Cannon, "Coded aperture imaging with uniformly redundant arrays," *Applied optics*, vol. 17, no. 3, pp. 337–347, 1978.

[5] A. Levin, R. Fergus, F. Durand, and W. T. Freeman, "Image and depth from a conventional camera with a coded aperture," in *ACM Transactions on Graphics (TOG)*, vol. 26, p. 70, ACM, 2007.

[6] A. Veeraraghavan, R. Raskar, A. Agrawal, A. Mohan, and J. Tumblin, "Dappled photography: Mask enhanced cameras for heterodyned light fields and coded aperture refocusing," *ACM Trans. Graph.*, vol. 26, no. 3, p. 69, 2007.

[7] J. Holloway, A. C. Sankaranarayanan, A. Veeraraghavan, and S. Tambe, "Flut-

ter shutter video camera for compressive sensing of videos," in *Computational Photography (ICCP), 2012 IEEE International Conference on*, pp. 1–9, IEEE, 2012.

[8] S. Tambe, A. Veeraraghavan, and A. Agrawal, "Towards motion aware light field video for dynamic scenes," in *Computer Vision (ICCV), 2013 IEEE International Conference on*, pp. 1009–1016, IEEE, 2013.

[9] P. Durrant, M. Dallimore, I. Jupp, and D. Ramsden, "The application of pinhole and coded aperture imaging in the nuclear environment," *Nuclear Instruments and Methods in Physics Research Section A: Accelerators, Spectrometers, Detectors and Associated Equipment*, vol. 422, no. 1, pp. 667–671, 1999.

[10] A. Olivo and R. Speller, "A coded-aperture technique allowing x-ray phase contrast imaging with conventional sources," *Applied Physics Letters*, vol. 91, no. 7, p. 074106, 2007.

[11] E. Caroli, J. Stephen, G. Di Cocco, L. Natalucci, and A. Spizzichino, "Coded aperture imaging in x-and gamma-ray astronomy," *Space Science Reviews*, vol. 45, no. 3-4, pp. 349–403, 1987.

[12] S. Huang and M. V. Hynes, "Coded aperture x-ray imaging system," Aug. 17 1999. US Patent 5,940,468.

[13] V. Dragoi, A. Filbert, S. Zhu, and G. Mittendorfer, "Cmos wafer bonding for back-side illuminated image sensors fabrication," in *Electronic Packaging Technology & High Density Packaging (ICEPT-HDP), 2010 11th International Conference on*, pp. 27–30, IEEE, 2010.

[14] J. Tanida, T. Kumagai, K. Yamada, S. Miyatake, K. Ishida, T. Morimoto, N. Kondou, D. Miyazaki, and Y. Ichioka, "Thin observation module by bound optics (TOMBO): concept and experimental verification," *Applied optics*, vol. 40, no. 11, pp. 1806–1813, 2001.

[15] M. Shankar, R. Willett, N. Pitsianis, T. Schulz, R. Gibbons, R. Te Kolste, J. Carriere, C. Chen, D. Prather, and D. Brady, "Thin infrared imaging systems through multichannel sampling," *Applied optics*, vol. 47, no. 10, pp. B1–B10, 2008.

[16] A. Brückner, J. Duparré, R. Leitel, P. Dannberg, A. Bräuer, and A. Tünnermann, "Thin wafer-level camera lenses inspired by insect compound eyes," *Optics Express*, vol. 18, no. 24, pp. 24379–24394, 2010.

[17] K. Venkataraman, D. Lelescu, J. Duparré, A. McMahon, G. Molina, P. Chatterjee, R. Mullis, and S. Nayar, "Picam: An ultra-thin high performance monolithic camera array," *ACM Transactions on Graphics (TOG)*, vol. 32, no. 6, p. 166, 2013.

[18] E. J. Tremblay, R. A. Stack, R. L. Morrison, and J. E. Ford, "Ultrathin cameras using annular folded optics," *Applied optics*, vol. 46, no. 4, pp. 463–471, 2007.

[19] A. Wang, P. Gill, and A. Molnar, "Angle sensitive pixels in cmos for lensless 3d imaging," in *Custom Integrated Circuits Conference, 2009. CICC'09. IEEE*, pp. 371–374, IEEE, 2009.

[20] P. R. Gill, C. Lee, D.-G. Lee, A. Wang, and A. Molnar, "A microscale camera using direct fourier-domain scene capture," *Optics letters*, vol. 36, no. 15, pp. 2949–2951, 2011.

[21] P. R. Gill and D. G. Stork, "Lensless ultra-miniature imagers using odd-symmetry spiral phase gratings," in *Computational Optical Sensing and Imaging*, pp. CW4C–3, Optical Society of America, 2013.

[22] D. Stork and P. Gill, "Lensless ultra-miniature cmos computational imagers and sensors," in *International Conference on Sensor Technologies and Applications*, pp. 186–190, 2013.

[23] A. Greenbaum, W. Luo, T.-W. Su, Z. Göröcs, L. Xue, S. O. Isikman, A. F. Coskun, O. Mudanyali, and A. Ozcan, "Imaging without lenses: Achievements and remaining challenges of wide-field on-chip microscopy," *Nature methods*, vol. 9, no. 9, pp. 889–895, 2012.

[24] A. Greenbaum, Y. Zhang, A. Feizi, P.-L. Chung, W. Luo, S. R. Kandukuri, and A. Ozcan, "Wide-field computational imaging of pathology slides using lens-free on-chip microscopy," *Science translational medicine*, vol. 6, no. 267, pp. 267ra175–267ra175, 2014.

[25] E. J. Candes, J. K. Romberg, and T. Tao, "Stable signal recovery from incomplete and inaccurate measurements," *Communications on pure and applied mathematics*, vol. 59, no. 8, pp. 1207–1223, 2006.

[26] D. L. Donoho, "Compressed sensing," *Information Theory, IEEE Transactions on*, vol. 52, no. 4, pp. 1289–1306, 2006.

[27] R. G. Baraniuk, "Compressive sensing," *IEEE signal processing magazine*, vol. 24, no. 4, 2007.

[28] R. F. Marcia and R. M. Willett, "Compressive coded aperture superresolution image reconstruction," in *Acoustics, Speech and Signal Processing, 2008.*

ICASSP 2008. IEEE International Conference on, pp. 833–836, IEEE, 2008.

[29] A. Wagadarikar, R. John, R. Willett, and D. Brady, "Single disperser design for coded aperture snapshot spectral imaging," *Applied optics*, vol. 47, no. 10, pp. B44–B51, 2008.

[30] P. Llull, X. Liao, X. Yuan, J. Yang, D. Kittle, L. Carin, G. Sapiro, and D. J. Brady, "Coded aperture compressive temporal imaging," *Optics express*, vol. 21, no. 9, pp. 10526–10545, 2013.

[31] A. Zomet and S. K. Nayar, "Lensless imaging with a controllable aperture," in *Computer Vision and Pattern Recognition, 2006 IEEE Computer Society Conference on*, vol. 1, pp. 339–346, IEEE, 2006.

[32] G. Huang, H. Jiang, K. Matthews, and P. Wilford, "Lensless imaging by compressive sensing," in *20th IEEE International Conference on Image Processing*, pp. 2101–2105, IEEE, 2013.

[33] M. J. DeWeert and B. P. Farm, "Lensless coded-aperture imaging with separable doubly-toeplitz masks," *Optical Engineering*, vol. 54, no. 2, pp. 023102–023102, 2015.

[34] S. W. Golomb *et al.*, *Shift register sequences*. Aegean Park Press, 1982.

[35] G. H. Golub and C. F. Van Loan, *Matrix computations*, vol. 3. JHU Press, 2012.

[36] L. I. Rudin, S. Osher, and E. Fatemi, "Nonlinear total variation based noise removal algorithms," *Physica D: Nonlinear Phenomena*, vol. 60, no. 1, pp. 259–268, 1992.

[37] S. Mallat, *A wavelet tour of signal processing: the sparse way.* Academic press, 2008.